Int. J. Electrochem. Sci., 13 **(2018)** 11974 – 11985, doi: 10.20964/2018.12.42

International Journal of ELECTROCHEMICAL SCIENCE
www.electrochemsci.org

A Simulation Study of the Direct Current Corrosion Characteristics of Carbon Steel Grounding Electrode with Ground Lead

Zhanlong Zhang[1,*], *Pan Gao*[1], *Yihua Dan*[1], *Guohua Liu*[2], *Rui Xiang*[1], *Jing Zou*[1]

[1] State Key Laboratory of Power Transmission Equipment & System Security and New Technology, Chongqing University, Chongqing, 400030, China
[2] Zhejiang Quzhou Power Supply Company of State Grid, Zhejiang, 324000, China)
[*]E-mail: zhanlongzhang@163.com

Received: 18 October 2017 / *Accepted:* 29 September 2018 / *Published:* 5 November 2018

In this study, corrosion of the horizontal linear carbon steel grounding electrode buried in soil of the transmission system at various direct current (DC) densities was investigated by the electrode potential, pH, anode iron dissolution and corrosion rate. A simulation model of DC corrosion behavior was established. The corrosion micro-mechanism of grounding electrode under DC interference was analyzed. This study found that the stray current density has a positive correlation with electrode potential, anode iron dissolution and corrosion rate. The DC current will significantly accelerate the dissolution rate and corrosion rate of the steel. The DC density has a different influence on the soil pH around the grounding electrode.

Keywords: Grounding electrode; Corrosion; Stray current; Simulation

1. INTRODUCTION

Grounding electrode is the main component of a grounding device and is used for current diffusion of power system towers and electrical devices to ensure the safe operation of power grid and power equipment. Q235 carbon steel is commonly used in terrestrial grounding electrode given the extensive and inexpensive source of carbon steel [1, 2]. Carbon steel grounding electrode buried in the soil will cause electrochemical corrosion [3-7]. The strong DC in transmission grounding electrode flows out the electrode into the soil, which directly impacts the service life of grounding electrode [4]. The risk of electric accident increases when corrosion is serious.

The influence of DC on the corrosion process of carbon steel has been reported extensively [8–16]. Several studies were conducted on the corrosion behavior of buried pipeline under DC interference [9–12]. The influence of stray DC on buried pipelines in soil is closely related to the

interference time and density of stray current; thus, the effect of stray current on corrosion rate increases over time [9]. The corrosion behavior of carbon steel in soil can be tested and experimental data can be obtained by weightless measurement, electrochemical test, electron microscopy, and XRD [12, 14]. Existing experimental data can be compared with the numerical simulation of the present study. Qian et al. [12] studied the corrosion characteristics of X52 steel pipeline in simulated soil solution at different DC densities. They found that DC accelerates the process of anode iron dissolution and considerably influences the integrity of the pipeline. DC can increase the pH level of a cathode, which may lead to the loss of surface coating of the pipeline. Similarly, Dai et al. [14] and Wen et al. [11] found that the corrosion rate of steel in the presence of DC is larger than that without DC; high amplitude of current density increases the rate of corrosion of steel. These studies show that the interference corrosion behavior of DC is closely related to current density. However, given the limitations of simulation technology, existing studies mainly focus on experimental measurement. Moreover, only a few studies examined the micro-mechanism and numerical simulation of the characteristics of DC corrosion of carbon steel in soil. Micro-mechanism research and numerical simulation play important roles in the prediction and evaluation of corrosion behavior.

This study simulated and analyzed the corrosion process of carbon steel grounding electrode at various DC current densities to investigate the corrosion characteristic of horizontal linear DC transmission grounding electrode. This study can provide theoretical guidance for the prediction, protection, and diagnosis of corrosion of DC transmission grounding electrode of carbon steel.

2. DC CORROSION PROCESS OF GROUNDING ELECTRODE

2.1 Natural corrosion process

Q235 carbon steel is commonly used in terrestrial grounding electrode to study of the grounding electrode of DC transmission. Table 1 shows the chemical composition of Q235. Carbon steel grounding electrode in soil environment occurs electrochemical reaction as shown in Formulas (1) and (2).

Anodic reaction (iron corrosion dissolution process):

$$Fe \rightarrow Fe^{2+} + 2e \quad (1)$$

Cathodic reaction (oxygen reduction reaction):

$$4O_2 + 2H_2O + 4e \rightarrow 4OH^- \quad (2)$$

Table 1. Chemical compositions of the carbon steel studied (wt. %)

Steel	C	Si	Mn	S	P	Cu	Fe
Q235	0.176	0.233	0.057	0.023	0.019	0.033	Balance

The Fe^{2+} produced in the anode and the OH^- produced in the cathode are diffused in the soil and combined to produce primary corrosion product $Fe(OH)_2$ as shown in Formula (3); $Fe(OH)_2$ in the case of sufficient oxygen will cause reaction as shown in Formula (4) [12]. Fe^{2+} prone to hydrolysis will also generate $Fe(OH)_2$, as shown in Formula (5).

$$Fe^{2+} + 2OH^- \rightarrow Fe(OH)_2 \quad (3)$$

$$4Fe(OH)_2 + O_2 \rightarrow 2Fe_2O_3 + 4H_2O \quad (4)$$

$$Fe^{2+} + 2H_2O \rightleftharpoons Fe(OH)_2 + 2H^+ \quad (5)$$

2.2 Material diffusion and electrochemical reactions

13 kinds of particles are considered in the corroding system, namely, OH^-, H^+, Na^+, Cl^-, SO_4^{2-}, Fe^{2+}, $Fe(OH)^+$, $Fe(OH)_2$, $FeCl^+$, $FeCl_2$, $FeCl_4^{2-}$, O_2, and H_2. The equilibrium formula of an ion *i* in soil solution is described in Formula (6).

$$\frac{\partial c_i}{\partial t} + \nabla \cdot \mathbf{N}_i = R_{i,tot} \quad (6)$$

Where $\mathbf{N}_i$ is the flux of ion *i* [SI: mol/(m$^2 \cdot$ s)]. The flux of ion *i* in the electrolyte can be expressed using the Nernst-Planck formula (7).

$$\mathbf{N}_i = \underbrace{-D_i \nabla c_i}_{Diffusion} \underbrace{-z_i u_{m,i} F c_i \nabla \phi_l}_{Mobility} + \underbrace{c_i \mathbf{u}}_{Convection} \quad (7)$$

The right side of the formula corresponds to the flux of charged ions by free diffusion, action of the electric field, and convection of the solution. In Formula (7), c_i is the concentration of ion *i* (unit: mol/m^3), z_i is the valence or charge number of the ion, D_i is the diffusion coefficient (unit: m^3/s), $u_{m,i}$ is the mobility (unit: s$\cdot$mol/kg), *F* is Faraday constant (unit: C/mol, its value is generally considered to be 96485.3383±0.0083 C/mol), φ_l is the electrolyte potential, $\mathbf{u}$ is convection speed (unit: m/s), and $u_{m,i}$ can be expressed as Nernst-Einstein relationship in Formula (8).

$$u_{m,i} = D_i / RT \quad (8)$$

Where D_i is the diffusion coefficient, the value of which can be obtained from Heppner [17] and Chang [18].

The equilibrium reactions involved in the corroding system and the equilibrium constant are shown in Table 2. Table 3 describes the electrochemical reactions.

Table 2. Equilibrium reactions and their equilibrium constants

Reaction	lgK_{eq}	References
$Fe^{2+} + H_2O \rightleftharpoons Fe(OH)^+ + H^+$	$K_1 = -8.3$	[19,20]
$Fe(OH)^+ + H_2O \rightleftharpoons Fe(OH)_2 + H^+$	$K_2 = -11.1$	[19,20]
$Fe^{2+} + Cl^- \rightleftharpoons FeCl^+$	$K_3 = -0.161$	[19,20]
$Fe^{2+} + 2Cl^- \rightleftharpoons FeCl_2$	$K_4 = -2.45$	[19,20]
$Fe^{2+} + 4Cl^- \rightleftharpoons FeCl_4^{2-}$	$K_5 = -1.90$	[19,20]
$H_2O \rightleftharpoons OH^- + H^+$	$K_6 = -14$	[19,20]

Table 3. Electrochemical reactions occurring at the corroding system

Description of reactions	Reaction	Current density (A/m2)	References
Reduction of water	$H_2O + 2e \rightarrow 2OH^- + H_2$	$i_{H2O} = -i^0_{H2O} 10^{\frac{\eta}{bH2O}}$	[21]
	$2H^+ + 2e \rightarrow H_2$	$i_{H2} = -i^0_{H2} 10^{\frac{\eta}{bH2}}$	[22]
Reduction of oxygen	$O_2 + H_2O + 4e \rightarrow 4OH^-$	$i_{O2} = -i^0_{O2} \frac{c_{O2}}{c_{O2,ref}} 10^{\frac{\eta}{bO2}}$	[22]
Oxidation of Fe	$Fe \rightarrow Fe^{2+} + 2e$	$i_{Fe} = i^0_{Fe} 10^{\frac{\eta}{bFe}}$	[22,23]

2.3 Micro-mechanism of DC corrosion of grounding electrode

When grounding current I_{in} flows to the grounding electrode, current I flows in the metal phase of the electrode caused by the internal movement of electrons or holes. The substance can obtain or lose electrons at the junction with the soil solution phase through electrochemical reactions to enable the current to flow out of the grounding electrode. The current flows through directional migration or diffusion of dissolved ions or charged particles in the soil solution. The conduction current I generated inside the grounding metal phase flows into the axial direction along the electrode, and the current flows out of the electrode to form stray current I_o. When the grounding current flows out of the grounding electrode, the lost electrons of anode iron atoms transform into ferrous ions and form anode current i_a. Similarly, hydroxide ions in the cathode were generated by the reaction of oxygen and hydrogen reduction to form cathode current i_c.

Kirchhoff law indicates that the grounding current that flows into the grounding electrode is equal to the sum of stray current flowing out of the grounding electrode surface. Stray current I_o is formed by the conversion of iron metal into iron ions. Therefore, the grounding current I_{in} is equal to the sum of the dissolved current, and the absolute value of the cathode current i_c is equal to the difference between the dissolution current i_a and the stray current I_o. The micro-mechanism of the DC corrosion process of grounding electrode is shown in Fig. 1.

Total current $\sum i_a$ produced by all anodic reactions on the surface of grounding electrode and the total current $\sum i_c$ produced by all cathodic reactions are related to stray current I_o as shown in Formula (9). The relationship between grounding current I_{in} and stray current I_o is shown in Formula (10).

$$\sum_1^n I_o = \sum_1^n i_a + \sum_1^n i_c \quad (9)$$

$$I_{in} = \sum_1^n I_o \quad (10)$$

Where the stray current I_o is generated by the grounding current that flowing out the grounding electrode surface. For the grounding electrode, it is an external current; I_{in} is the grounding current flowing into the grounding electrode by the ground lead; i_a is the anode current generated by electrochemical corrosion of iron metal. It is generated by localized corrosion reactions; and i_c is the cathode current generated by the cathodic reaction of electrochemical corrosion. It is generated by localized corrosion reactions.

Therefore, Formulas (9) and (10) for the corrosion of carbon steel grounding electrode in soil solution can be expressed as Formula (11).

$$I_{in} = i_{Fe} + i_{O_2} \tag{11}$$

Formula (11) shows the relationship between the grounding current and the total current generated by cathodic and anodic reactions; i_{Fe} and i_{O_2} are the total currents of anode and cathode, respectively.

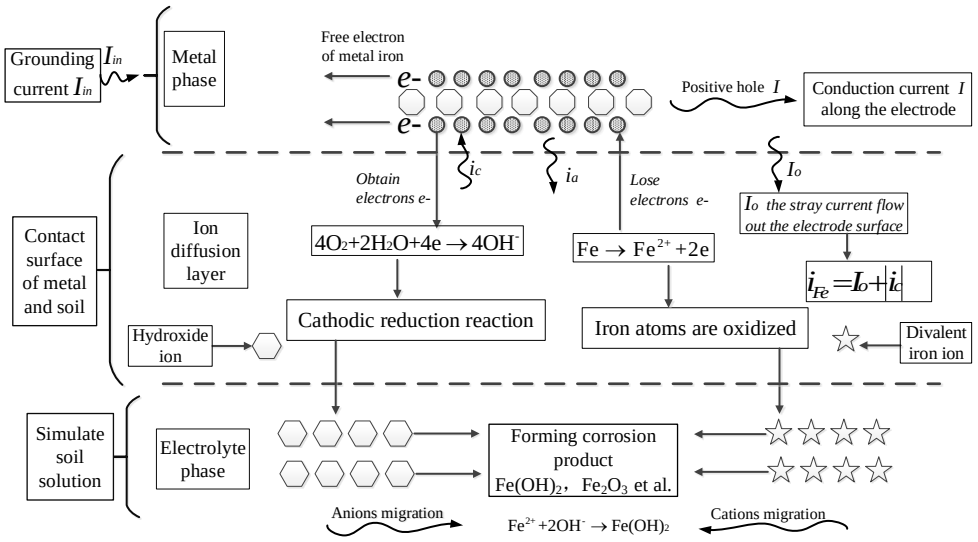

Figure 1. Micro-mechanism of DC corrosion process of the grounding electrode

2.4 Corrosion dissolution

The dissolution rate of the iron is related to the anodic reaction when the grounding electrode is in the natural corrosion state. According to Faraday's law, the relationship between the local current and the flux density produced by electrochemistry is given by Formula (12).

$$R_{j,m} = \frac{-v_{j,m} i_{loc,m}}{n_m F} \tag{12}$$

Where j is the dissolved substance, m is the reaction involved in the dissolved substance, and $v_{j,m}$ is the number of substances involved in the reaction of the dissolved substance, which can be an integer or a fraction. The symbol is positive to indicate that the substance is dissolved. $i_{loc,m}$ is the local current generated by the electrochemical reaction, and n_m is the number of electrons involved in the reaction that is constantly positive.

In natural corrosion, local current $i_{loc,m}$, cathode current i_c, and anode current i_a satisfy Formula (13).

$$i_{loc,m} = i_{Fe} = |i_c| \tag{13}$$

When the grounding current flows through the grounding electrode, the conduction current flows out of the grounding electrode surface to the soil, which changes the value of $i_{loc,m}$. For a particular point on the grounding electrode surface, the local current $i_{loc,m}$ can be expressed as Formula (14).

$$i_{loc,m} = i_{Fe} = I_o + |i_c| \tag{14}$$

The flux of divalent iron ions is determined by the dissolution rate of iron. The dissolution rate can be expressed as Formula (15).

$$\mathbf{n} \cdot \mathbf{v} = \sum_j \sum_m \frac{R_{j,m} M_j}{\rho_j} = -\frac{i_{loc,Fe} M_{Fe}}{n_m F \rho_{Fe}} = -(I_o + |i_c|) \frac{M_{Fe}}{n_m F \rho_{Fe}} \tag{15}$$

Where M_j is the molar mass of the dissolved substance (the molar mass of Fe is 0.056 kg/mol), and ρ_j is the density of the dissolved metal (the density of Fe is 7800 kg/m^3).

3. RESULTS AND DISCUSSION

In this paper, simulation calculations are implemented using finite element software COMSOL Mutiphysics. In COMSOL Multiphysics there is a special electrochemical corrosion module called Tertiary Current Distribution Nernst-Planck. The electrochemical corrosion process can be simulated and calculated by this module. Time Dependent with Initialization is selected in the study section. In the Tertiary Current Distribution Nernst-Planck window, locate the Electrode Surface section to set the anode and cathode parameters of the electrochemical reactions. For natural corrosion, the sum of the total current at the Electrode Surface boundary is 0. When an external current such as grounding current is injected to the electrode, the corresponding Electrode Surface boundary current value should be reset.

The numerical simulation in this study is compared with the experimental results of Qian [12]; their experimental model is described in the following statements. A long straight steel electrode is placed in simulated soil solution. A 10 mm × 10 mm steel sample is located above the steel electrode with cathodic protection. The current densities in the soil solution along the axial direction of the steel electrode were 0.1 A/m^2, 0.5 A/m^2, 1 A/m^2, 2 A/m^2, 5 A/m^2, and 10A/m^2. External DC flows into the solution to form a stray DC. The authors measured parameters, such as electrode potential, pH, and corrosion rate of the steel electrode at time 1200s, under natural condition and at various current densities, respectively.

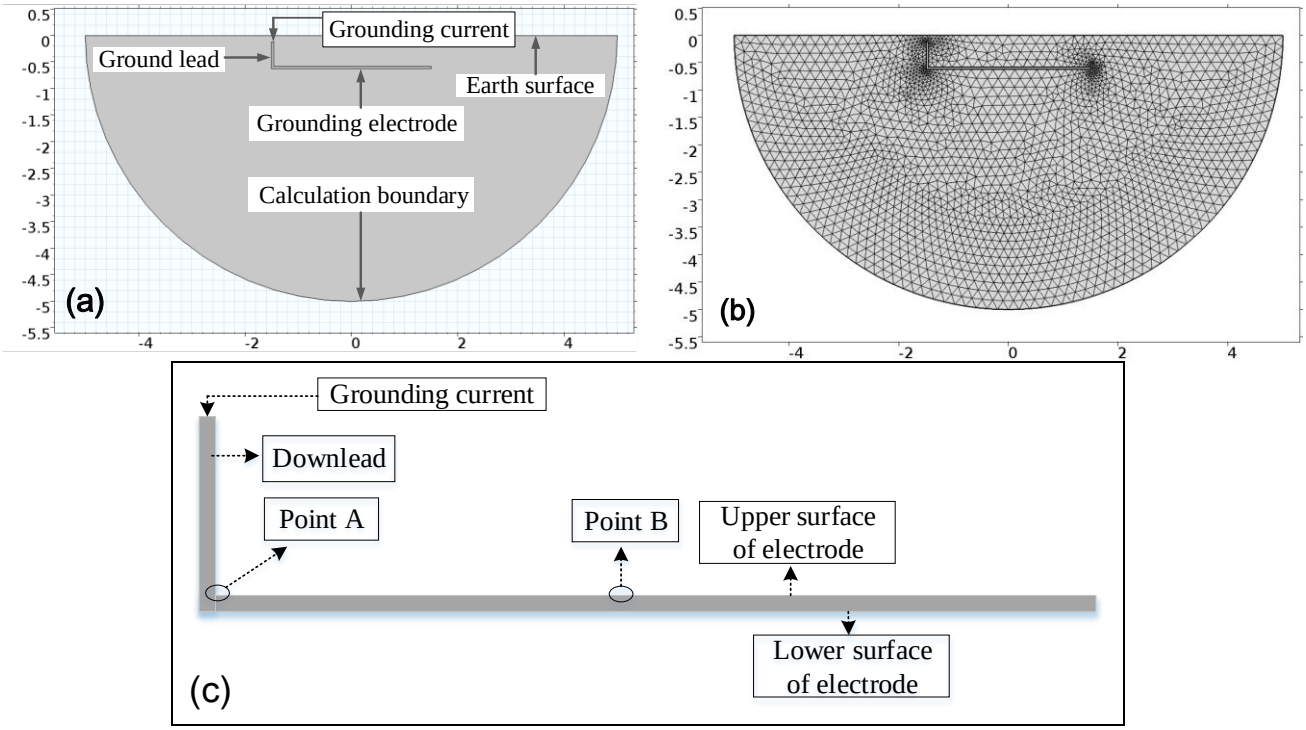

Figure 2. Geometric model for calculation (a) Two-dimensional graphic; (b) Mesh subdivision; (c) Calculation points and boundary

The numerical simulation model in this study is described as follows. Fig. 2(a) shows the hemispherical simulated soil solution with radius of 5 dm. The horizontal grounding electrode length is 3 dm, radius of electrode is 0.02 dm, buried depth is 0.6 dm, ground lead length is 0.5 dm, and the corresponding radius is 0.02 dm. The space position of the grounding electrode is symmetrical. Thus, the three-dimensional space calculation can be simplified to two-dimensional. The calculated mesh pattern is shown in Fig. 2(b). Points A and B of the grounding electrode shown in Fig. 2(c) are selected as objects of study. The electrode potential, iron dissolution, electrode thickness change and corrosion rate at various DC stray current densities (0.1 A/m^2, 0.5 A/m^2, 1 A/m^2, 2 A/m^2, and 5 A/m^2) were calculated. Corrosion time was 1200 s.

3.1 Potential of the electrode in soil solution at various stray current densities

Point A in Fig. 2(c) was selected as analysis object. The electrode potential of point A at various DC densities are shown in Fig. 3(a).

Electrode potential increases as the DC stray current density increases. The anode potential of the experimental model of S. Qian is compared with the numerical simulation in Fig. 3(b). The potential variation tendency is similar, the simulation result is slightly larger than the experimental result. The reason for this error is that due to the presence of stray current in the soil solution of experimental model, the actual current density flowing out the surface of steel material is slightly reduced. In the simulation model, this phenomenon is negligible due to the presence of the ground lead. Fig. 3(c) and (d) Figure 2 shows the change in electrode potential over time when the stray current density is 0A/m^2 and 1A/m^2, respectively. The change in electrode potential over time is very

small, so the electrode potential distribution shown in Fig. 3(a) exhibits an approximately constant value.

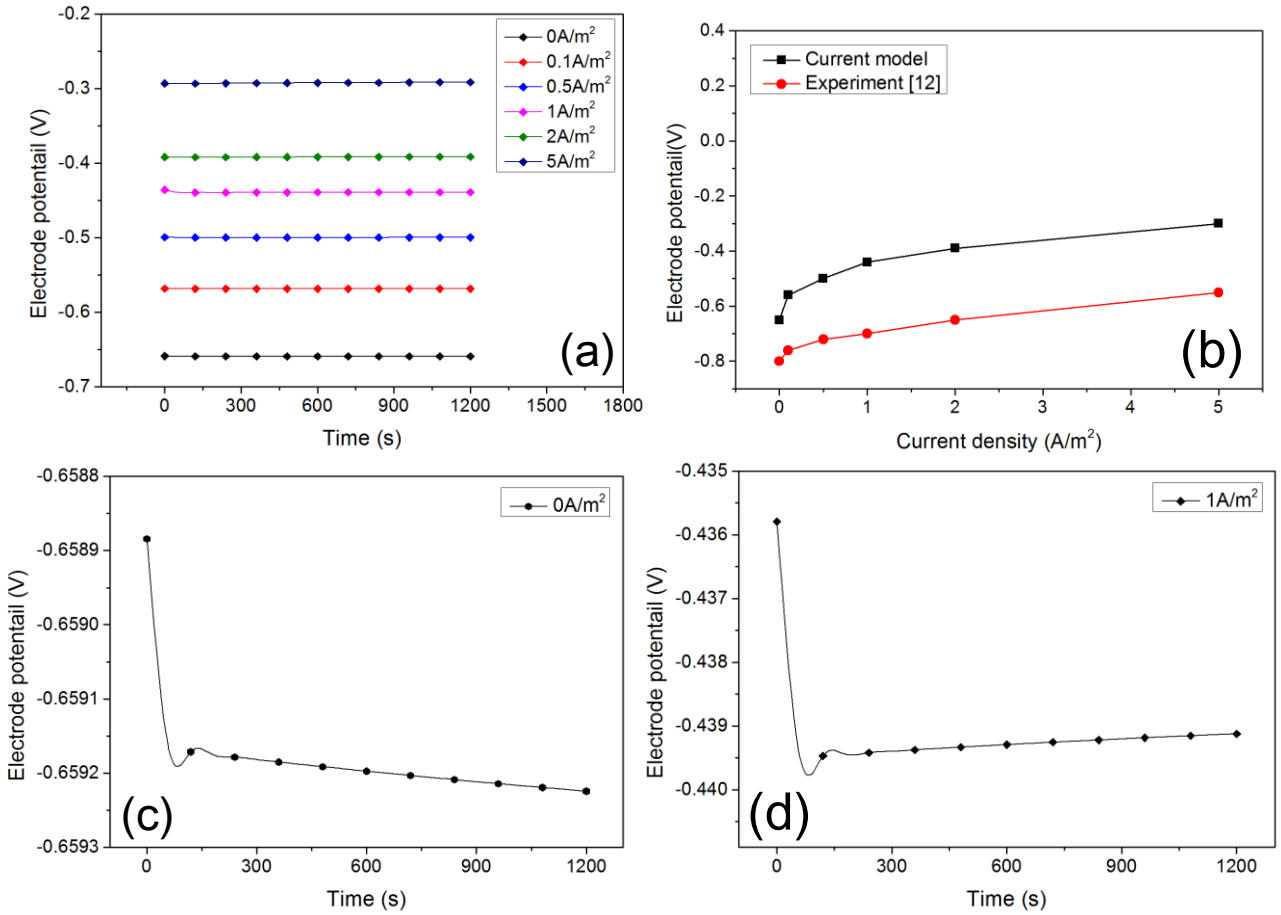

Figure 3. Electrode potential at various DC densities (a) Electrode potential; (b) comparison; (c) 0A/m^2; (c) 1A/m^2

3.2 Solution pH near the grounding electrode surface

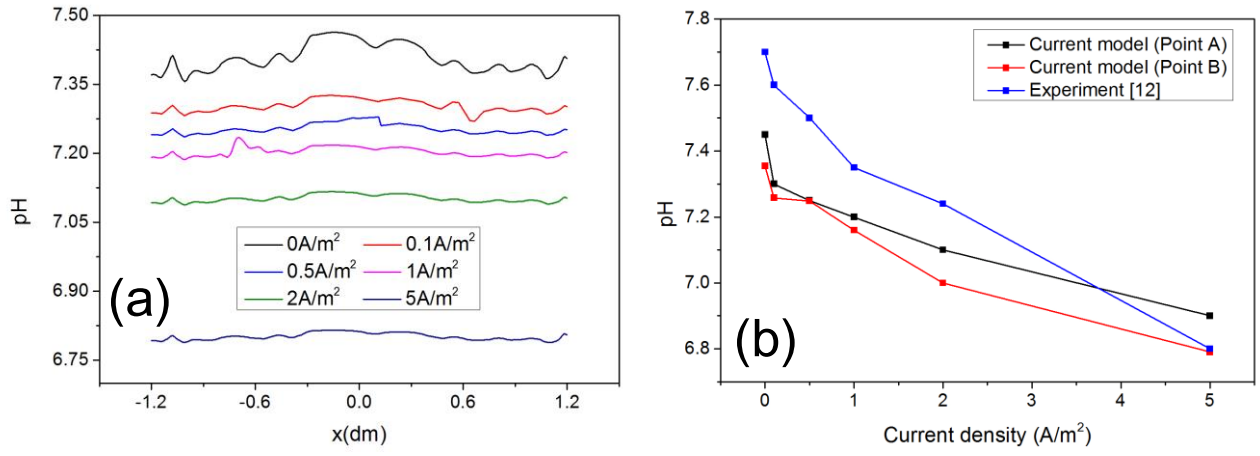

Figure 4. The pH (a) The pH distribution at various DC densities; (b) comparison

The pH distribution of the soil at a distance of 0.03 dm from the top surface of the grounding electrode is shown in Fig. 4(a) when the corrosion proceeds to 1200 s. The comparison of the pH values near the points A and B at various DC densities with experimental measurement data is shown in Fig. 4(b). It can be seen from the figure that the simulation results and the experimental results are basically close, and the simulation results can also better describe the pH of the solution near the surface of the corrosion metal, and can provide a certain reference for the actual metal corrosion.

3.3 Anode iron dissolution and electrode thickness change

Dissolution rate is a variable that describes the electrochemical reaction rate of the anodic iron. The anode iron dissolution rate is an important variable to describe the steel corrosion because the dissolution rate and corrosion rate are directly proportional as shown in formula (12) and (15).

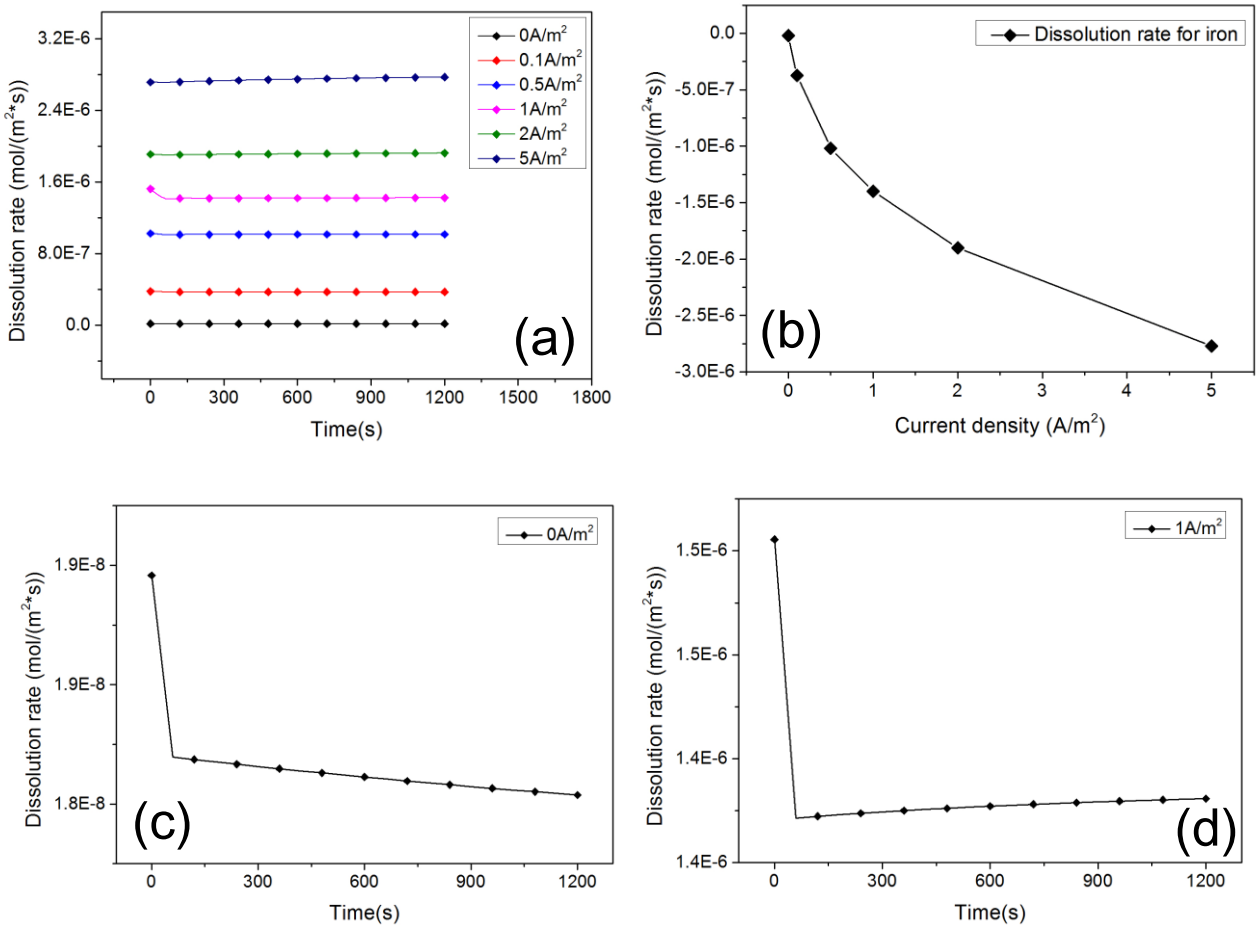

Figure 5. Iron dissolution rate and electrode thickness change of point A(a) The relationship between iron dissolution rate and time (b) The relationship between dissolution rate and current density; (c) 0A/m^2; (d) 1A/m^2

The anode iron dissolution rate and electrode thickness change at point A are analyzed. Fig. 5 and Fig. 6 show the change of the iron dissolution rate and electrode thickness of point A with time, respectively, at various DC densities. The anode iron dissolution rate and electrode thickness change at various current densities with time is shown in Fig. 5(a) and Fig. 6(a). Fig. 5(b) and Fig. 6(b) show the

relationship of iron dissolution rate and electrode thickness change of point A at various DC densities, when the corrosion proceeds to 1200 s. The anode iron dissolution rate gradually increased with the increase of DC density, and the DC substantially influenced the anode process by accelerating iron dissolution. As shown in Fig. 6, the change in the electrode thickness at point A increased and the dissolution of the anode iron resulted in a decrease in the volume of the grounding electrode and damaged structural integrity. The actual metal surface area is reduced, which limits the current diffusion of grounding electrode.

In addition, the relationship between iron dissolution rate and time is shown in Fig. 5(c) and (d). As can be seen from the Figures, the change in dissolution rate over time is very small, so the dissolution rate distribution shown in Fig. 5(a) exhibits an approximately constant value. The thickness change of the electrode is caused by the corrosion dissolution of iron, and the greater the DC density, the greater the dissolution rate.

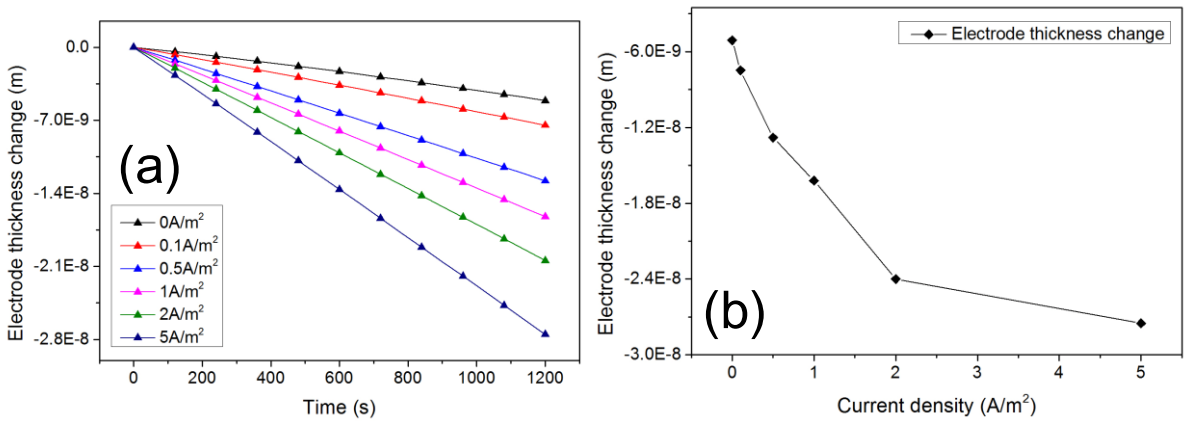

Figure 6. Electrode thickness change (a) The relationship between electrode thickness change and time; (b) the relationship between electrode thickness change and DC current density

3.4 Corrosion rate at various DC current densities

Corrosion rate is a variable that can directly describe the speed of metal corrosion. Formula (15) describes the relationship between the DC current and the corrosion rate. Corrosion rate refers to the average corrosion degree of per unit time. The corrosion rate unit in this paper adopts mm/year. Current research shows that DC can significantly accelerate the corrosion rate of steel materials, thereby accelerating the damage to the steel structure [9,11,12,14,26]. After injecting 0.2A~1.6A current into two carbon steel materials Q235 and Q345 respectively, He et al. [26] found that with the increase of the injected current amplitude, the corrosion rate of the carbon steel material gradually increases, and the corrosion rate shows a positive correlation with the direct current. Qian [12] also obtained the same conclusion. The relationship between the DC current and the corrosion rate is shown in Fig. 7(b). The results of this study on the effect of DC current on the corrosion rate of steel materials are shown in Figure 7. The numerical simulation results and the experimental results of the reference [12] are basically similar and the error is very small, which shows that the simulation research in this paper has a high accuracy. Figs. 7(a) shows the relationship of corrosion rate at point A at different DC current densities with time. The corrosion rate in the current model and measured in the experiment of

S. Qian when the corrosion proceeds to 1200s is shown in Fig. 7(b). Combining Figs. 5(a) and 7(a) shows that the dissolution rate of the anode iron was positively correlated with the corrosion rate. The corrosion rate gradually increases as the DC grounding current density increases. Fig. 7(b) also shows that the corrosion rate increases as the grounding current density increases, and the variation tendency is consistent with the experiment data of [12].

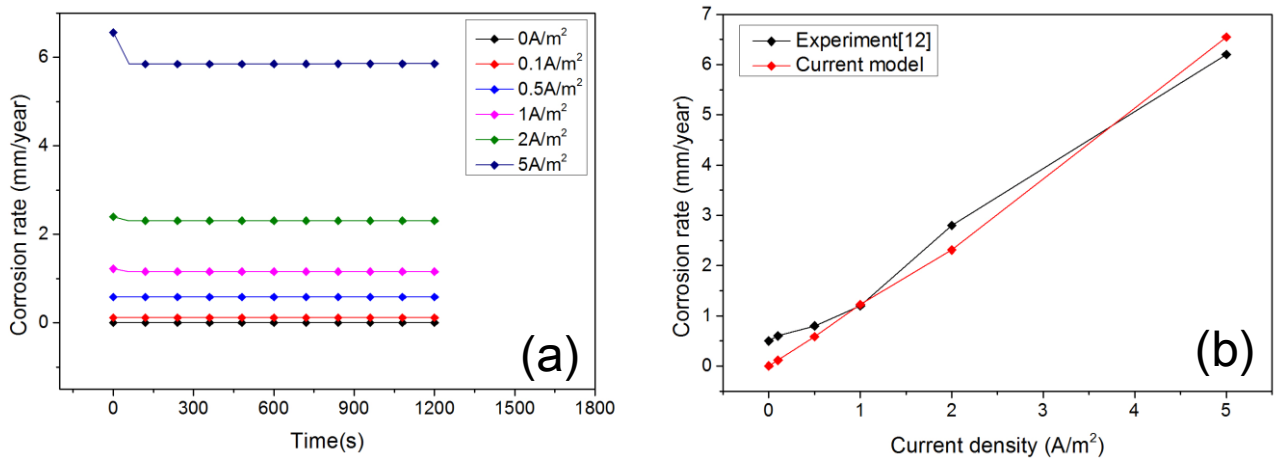

Figure 7. Corrosion rate (a) Relationship between corrosion and time (b) Corrosion rate compared with experiment

4. CONCLUSION

This study established a corrosion model of carbon steel grounding electrode at various DC densities by studying the microscopic mechanism. The corrosion model is simulated by COMSOL Multiphysics. The influence of DC stray current on the electrode potential, pH, iron dissolution and corrosion rate were analyzed. The numerical simulation results was compared with the experimental results of S. Qian, the results prove that the simulation results have a very high degree of accuracy, and it is of great significance to study the DC corrosion characteristics of steel materials. Specific findings are listed below.

1. DC stray current affects electrode potential, that is, the greater the DC density, the higher the electrode potential. Electrode potential is shifted positively.

2. The soil pH around the grounding electrode is affected by the direct current, and the injection of external DC leads to an increase in the concentration of hydrogen ions.

3. DC stray current can accelerate the dissolution rate of the anode iron and the change rate of the electrode thickness. Higher stray current density will result in faster anode dissolution rate, larger change in electrode thickness, and faster corrosion rate of grounding electrode.

ACKNOWLEDGEMENTS
This work is supported by the National Natural Science Foundation of China [grant number 51577017].

References

1. Y.P. Shao, A.J. Yan, B. Li, Q.Q. Liao, *Corrosion Science and Protection Technology*, 04(2015)333.
2. A.J. Yan, B. Deng, J.H. Fu, P. Ma, *Shaanxi Electric Power*, 41(2013)65.
3. Y.Q. Li, C.W. Du, H. Feng, Y. Zhao, *Environmental Technology*, 28(2010)15.
4. W. Zhang, H. Li, Sui X, J. Guo, J. Yu, X. Wang, *Corrosion Science & Protection Technology*, 29(2017)80.
5. Z.Y. Qian, Z.P. Yu, *High Voltage Engineering*, 03 (1995)40.
6. S. Wang, Y.B. Hu, Z.Z. Li, S.J. Gao, H.L. Ji, C.F. Dong, X.G. Li, *Corrosion*, 12(2013)357.
7. F.J. Yan, X.G. Li, *Shandong Electric Power*, 01(2007)9.
8. J.F. Yu, M. Zhang, *Materials Protection*, 48(2015)14.
9. Y.X. Zhang, Y.X. Du, M.X. Lu, *Corrosion & Protection*, 34(2013)771.
10. S.S. Chen, L.J. Zhang, A.H. Yang, *Gas &Heat*, 23(2003)435.
11. C. Wen, J. Li, S. Wang, Y. Yang, *J. Nat. Gas Sci. Eng.*, 27(2015)1555.
12. S. Qian, Y.F. Cheng, *Constr. Build. Mater.*, 148(2017)675.
13. Z.G. Tan, Z.P. Zhu, F. Pei, J. Fu, X. Tian, B. Zeng, *Corrosion Science and Protection Technology*, 25(2013)207.
14. N. Dai, Q. Chen, J. Zhang, X. Zhang, Q.Z. Ni, Y.M. Jiang, J. Li, *Mater. Chem. Phys.*, 192 (2017)190.
15. Y.J. Weng, Y.Y. Li, C.C. Han, X.Y. Li, *Corrosion Science & Protection Technology*, 22(2010)01.
16. Y.J. Weng, Y.Y. Li, X.Y. Li, C.C. Han, *Corrosion Science & Protection Technology*, 21(2010)98.
17. K.L. Heppner, R.W. Evitts, P. John, *Can. J. Chem. Eng.*, 80(2010)857.
18. H.Y. Chang, Y.S. Park, W.S. Hwang, *J. Mater. Process. Tech.*, 103(2000)206-217.
19. H.Y. Chang, Y.S. Park, W.S. Hwang, *Metals & Materials*, 04(1998)1199.
20. W. Sun, L. Wang, T. Wu, G. Liu, *Corros. Sci.*, 78(2014)233.
21. F.M. Song, N. Sridhar, *Corros. Sci.*, 50(2008)70.
22. W. Wang, H.Y. Sun, L.J. Sun, Z.W. Song, B.N. Zang, *Chem. Res. Chin. Univ.*, 26(2010)822.
23. E.B. Muehlenkamp, M.D. Koretsky, J.C. Westall, *Corrosion*, 61(2012)519.
24. E. Stein, R.D. Borst, T.J.R. Hughes, *Encyclopedia of Computational Mechanics*, 03(2004)325-406.
25. J. Wu, H. Wang, X. Chen, P. Cheng, G.F. Ding, X.L. Zhao, Y. Huang, *Electrochim. Acta*, 75(2012)94.
26. Z.Q. He, X.J. Chen, H.F. Huang, Q.Q. Liu, *Electric Power Construction*, 32(2011)91.